SLIP-STACKING DYNAMICS AND THE 20 Hz BOOSTER

J. Eldred, Department of Physics, Indiana University, Bloomington, IN 47405, USA
R. Zwaska, FNAL, Batavia, IL 60510, USA

Abstract

Slip-stacking is an accumulation technique used at Fermilab since 2004 which nearly doubles the proton intensity. The Proton Improvement Plan II intensity upgrades require a reduction in slip-stacking losses by approximately a factor of 2. We introduce universal area factors to calculate the available phase space area for any set of beam parameters without individual simulation. We show the particle loss as a function of time and slip-stacking resonances. We calculate the injection efficiency as a function of longitudinal emittance and aspect-ratio. We demonstrate that the losses from RF single particle dynamics can be reduced by a factor of 4-10 (depending on beam parameters) by upgrading the Fermilab Booster from a 15-Hz cycle-rate to a 20-Hz cycle-rate. We recommend a change in injection scheme to eliminate the need for a greater momentum aperture in the Fermilab Recycler.

INTRODUCTION

Slip-stacking is integral to high-intensity operation at Fermilab and will play a central role in upgrades to the accelerator complex [1–3]. the Fermilab Proton Improvement Plan-II [1] calls for an improvement in beam power from 700 kW (with slip-stacking) to 1.2 MW with an eye towards multi-MW improvements. The increase in proton intensity requires a commensurate decrease in the slip-stacking loss-rate to limit activation in the tunnel. Single-particle dynamics associated with slip-stacking contribute directly to the particle losses. Our numerical results completely characterize the stable phase-space boundary and expresss this information as limits on the Booster beam quality. We show that including a 20-Hz Booster cycle-rate in the PIP-II upgrade relaxes the limits on the Booster beam quality and cuts particle losses due to slip-stacking.

BACKGROUND

Slip-stacking is a particle accelerator configuration that permits two high-energy particle beams of different momenta to use the same transverse space in a cyclic accelerator. The two beams are longitudinally focused by two sets of rf cavities with a small frequency difference between them. Each frequency is tuned to the momentum of one of the beams.

The two azimuthal beam distributions are manipulated as a consequence of their difference in rf frequency. Figure 1 shows the slip-stacking accumulation process. The two beams injected on separated portions of azimuth with a small frequency difference and overlap gradually, allowing injection [4]. When the cyclic accelerator is filled and the azimuthal distribution of the two beams coincide then the two beams are accelerated together by RF cavities operating at the average frequency. The potential beam intensity of a synchrotron is doubled through the application of this technique.

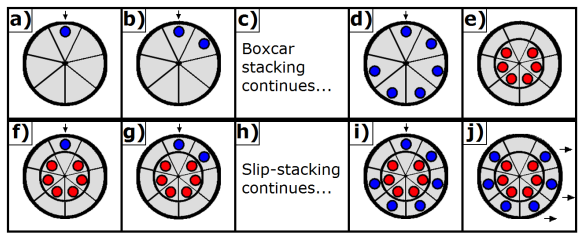

Figure 1: The Booster batch is represented by the circles and the Recycler (or Main Injector) is represented by the seven-sector wheel. **a)** The first batch is injected into the ring. **b)** One Booster cycle later the second batch is injected in the azimuthal space immediately behind the first batch. This is known as boxcar stacking. **c, d)** Boxcar stacking injections continue until six Booster batches are stored in the ring. **e)** The RF frequency is adiabatically lowered in between the sixth and seventh batch injection. **f)** The seventh batch is injected in the gap left by the previous six batches. Both cavities are operating at different frequency (slip-stacking). The first RF cavity matches the first six batches and the second RF cavity matches the next set of batches. **g)** One Booster cycler later the eighth batch is boxcar stacked with respect to the seventh batch but the frequency difference allows the injection to occur in the gap left by the first six batches. **h, i)** Slip-stacking injections continue until twelve Booster batches are stored in the ring. **j)** One Booster cycle later the kicker gaps of the first six and last six batches are aligned. At that time the batches are extracted to the Main Injector (if needed) and both beams are accelerated as one.

A preliminary study explored the beam dynamics in a 2-rf system [5]. The slipping of bunched beams was first demonstrated at the CERN SPS [6] but the emittance growth led to unacceptable particle losses. Fermilab has subsequently implemented slip-stacking operationally since 2004 [4, 7, 8]. Initially, the higher beam intensity was used to increase antiproton production for proton-antiproton collider experiments [9]. Subsequently, slip-stacking was applied to neutrino production for Neutrinos at Main Injector (NuMI) experiments [10–12].

Beam-loading effects can impact the effectveness of slip-stacking and were addressed in the Main Injector by the development of a beam-loading compensation system with -14dB feedback and -20dB feedforward [13–15]. The beam-loading effects on slip-stacking in the Recycler will be an order of magnitude weaker than in the Main Injector and

ISBN 978-3-95450-173-1

Table 1: Recycler and Booster Parameters Used in Analysis

Recycler Kinetic Energy (E)	8 GeV
Recycler Reference RF freq. (f)	52.8 MHz
Recycler Harmonic number (h)	588
Recycler Phase-slip factor (η)	-8.6*10^{-3}
Maximum Recycler RF Voltage (V)	2×150 kV
Booster harmonic number (h_B)	84
Booster cycle rate (f_B)	15/20 Hz
Difference in Recycler RF freq. (Δf)	1260/1680 Hz
Nom. Booster emittance ($\epsilon_{97\%}$)	0.12 eV·s
Nom. Booster Aspect Ratio	3.00 MeV/ns
Nom. Recycler Aspect Ratio (100 kV)	1.06 MeV/ns
Nom. Recycler Aspect Ratio (57 kV)	0.80 MeV/ns

can be compensated if necessary. The typical beam-loading voltage is ∼2kV [14] compared to a typical rf cavity voltage of 90kV [15]. In the Main Injector the R_{sh}/Q of the rf cavities is 100Ω [14], while in the Recycler the R_{sh}/Q is 13Ω [16]. This paper focuses on the constraints on the stable phase-space area fro

As Fig. 1 shows, the slipping rate of the buckets must be properly synchronized to the injection rate of new batches. The difference between the two RF frequencies must be equal to the product of the harmonic number of the Booster RF and the cycle rate of the Fermilab Booster. So for a Booster with a 15-Hz cycle-rate we have

$$\Delta f = h_B f_B = 84 \times 15 \text{ Hz} = 1260 \text{ Hz}$$

and for the proposed 20-Hz cycle-rate

$$\Delta f = h_B f_B = 84 \times 20 \text{ Hz} = 1680 \text{ Hz}.$$

The difference in the frequency of the two RF cavities is related to the difference in momentum of the two beams by:

$$\Delta\delta = \frac{\Delta f}{f_{rev} h \eta} \tag{1}$$

where h is the harmonic number of the Recycler and η is the phase-slip factor of the Recycler (see Table 1). Consequently, the momentum difference between the two beams is 0.28% for the 15-Hz Booster and 0.37% for the 20-Hz Booster.

A 20-Hz Booster also reduces the time required to accumulate 12 batches in the Recycler, making more beam available for 8-GeV experiments [17–19]. For example, a 1.333 s MI cycle time would consume 9 Hz of the Booster's cycles, the additional available 8-GeV beam would increase from 6 Hz to 11 Hz. Furthermore, if the Main Injector ramp cycle is shortened to extract protons for LBNE at 60 GeV [20], then a 20-Hz Booster could deliver more beam to LBNE than a 15-Hz Booster.

SLIP-STACKING PARAMETER AND STABILITY MAPS

The equations of motion for a single particle under the influence of two rf cavities with identical voltage and different frequencies are

$$\dot{\phi} = 2\pi f_{rev} h \eta \delta$$
$$\dot{\delta} = f_{rev} V_\delta [\sin(\phi) + \sin(\phi - \Delta f t)]. \tag{2}$$

where V_δ is the maximum change in δ during a single revolution[1] and Δf is the frequency difference between the two RF cavities.

This is an explicitly time-dependent system which is the subject of ongoing research in dynamical mathematics [21, 22]. Broadly speaking, slip-stacking is complicated by the fact that the two RF systems will interfere and reduce the stable bucket area. The further the buckets are away from each other in phase-space, the less interference there is. To quantify this, the literature [5–7, 21] has identified the importance of the slip-stacking parameter

$$\alpha_s = \frac{\Delta f}{f_s} \tag{3}$$

as the criterion for effective slip-stacking. Δf is the frequency difference between the two RF cavities and f_s is the single-RF synchrotron frequency $f_s = f_{rev}\sqrt{\frac{Vh|\eta|}{2\pi\beta^2 E}}$.

In fact, all nontrivial dynamics of slip-stacking depend only on α_s. For example, if one slip-stacking configuration has RF frequency separation $\Delta f = 15$ Hz and another configuration with the same α_s has RF frequency separation $\Delta f' = 20$ Hz then the second phase space diagram is isomorphic to the first where the δ axis must be scaled by $\Delta f'/\Delta f = 4/3$.

The greater the slip-stacking parameter α_s, the less the buckets interfere. Increasing the synchrotron frequency f_s by increasing the voltage will increase the bucket height, but also increase the interference. So, for a fixed frequency difference Δf, there is a tradeoff encountered when tuning the voltage for maximum phase-space area. To optimize the bucket area more precisely, we must simulate the single particle dynamics. Fortunately we can use the slip-stacking parameter to simplify the parameter space.

We create a stability map for each value of the slip-stacking parameter α_s. We map the stability of initial particle positions by integrating the equations of motion for each initial position. Each position is mapped independently and only the single particle dynamics are considered. The integration is iterated for 100 synchrotron periods. The stability of the particle is tested after every phase-slipping period. A particle is considered lost if its phase with respect to each of the first RF cavity, the second RF cavity, and the average of the two RF cavities, is larger than a certain cut-off (we used $3\pi/2$). Figure 2 shows an example of such a stability map; the large stable regions at the top-center and bottom-center are the buckets used for slip-stacking and the interference effect is clearly evident.

[1] $V_\delta = \frac{eV}{\beta^2 E}$, where V is the effective voltage of the RF cavity, e is the charge of the particle, $\beta = v/c$ is the velocity fraction of the speed of light, E is the total energy of the particle.

ISBN 978-3-95450-173-1

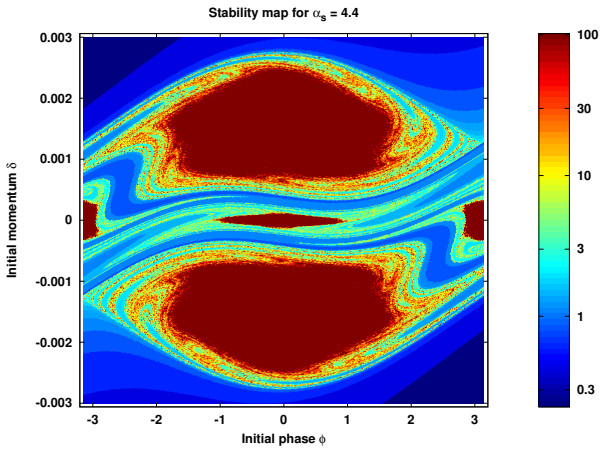

Figure 2: Stability of initial coordinates for $\alpha_s = 4.4$. The color corresponds to the number of synchrotron periods a particle with the corresponding initial coordinates survives before it is lost. The two large stable regions correspond to the higher and lower RF buckets where beam is injected and maintained.

We find some trajectories are "metastable" because they lead to particle loss only after thousands of revolutions. The stable phase-space area as a function of time is shown in Fig. 3 for several values of α_s. The loss of metastable phase-space area occurs at a rater that is faster than exponential decay.

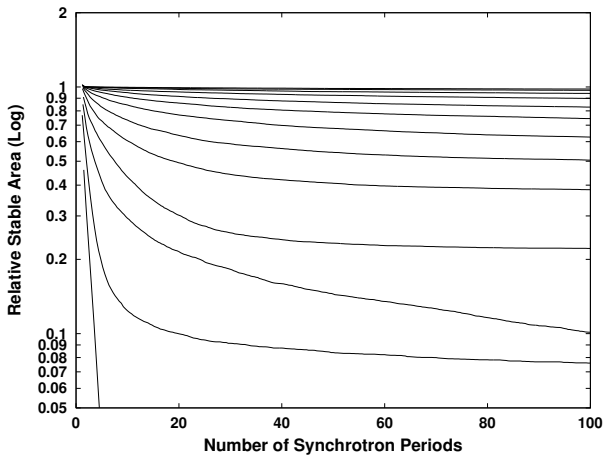

Figure 3: The stable area of the slip-stacking bucket relative to a single rf bucket, is plotted on a log scale and plotted over time. Each curve corresponds to a simulation with a different value of α_s with α_s = 2.0, 2.5, 3.0, 3.5, 4.0, 4.5, 5.0, 5.5, 6.0, 6.5, 7.0, 7.5, 8.0 (going from the bottom line to the top line).

The bucket area is computed as the product of the total number of ultimately surviving points and the cell area. We define the slip-stacking area factor $F(\alpha_s) = \mathcal{A}_s/\mathcal{A}_0$ as the ratio of the slip-stacking bucket area to that of a single-rf bucket with the same rf voltage and frequency. Then the phase space area ($\phi \cdot \delta$ units) can be expressed in terms of this factor $F(\alpha_s)$:

$$\mathcal{A}_s = \mathcal{A}_0 F(\alpha_s) = \frac{16}{h|\eta|}\frac{f_s}{f_{rev}}F(\alpha_s). \quad (4)$$

Figure 4(a) plots the numerically derived slip-stacking area factor $F(\alpha_s)$. Using Fig. 4(a) with Eq. 4 provides the first method for calculating the slip-stacking stable phase-space area without requiring each case to be simulated individually. $F(\alpha_s)$ increases rapidly above $\alpha_s \approx 3$ and asymptotically approaches 1. $F(\alpha_s)$ has several local minimum where resonances are crossed; this loss of area occurs when large amplitude trajectories have a parametric resonance and therefore does not occur at precise integer values of α_s.

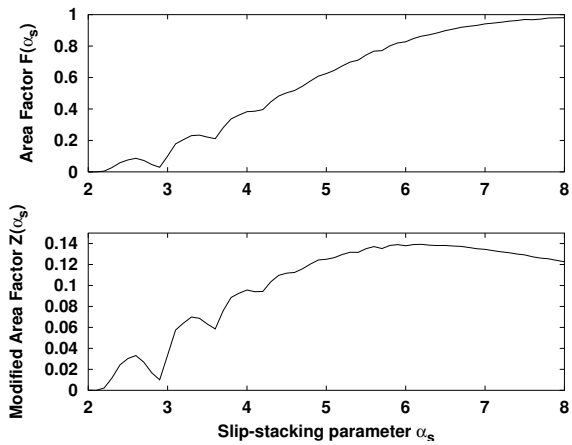

Figure 4: (a) The slip-stacking area factor as a function of α_s. As α_s increases the distance between the rf buckets becomes greater, the buckets become more independent, and the slip-stacking bucket area approaches the single-rf bucket area. (b) The modified slip-stacking area factor as a function of α_s. The modified slip-stacking area factor is maximized near $\alpha_s = 6.2$.

For a given Booster cycle-rate, the slip-stacking parameter α_s can be tuned by changing the RF voltage. The synchrotron frequency f_s which is proportional to the square root of the applied RF voltage and changes the bucket area by both the slip-stacking area factor $F(\alpha_s)$ and the single-rf bucket area. To identify the optimal voltage, we rewrite Eq. 4 to separate the parameters that are held constant from those dependent on α_s:

$$\mathcal{A}_s = \frac{16}{h|\eta|}\frac{\Delta f}{f_{rev}}\left(\frac{F(\alpha_s)}{\alpha_s}\right) = \frac{16}{h|\eta|}\frac{\Delta f}{f_{rev}}Z(\alpha_s). \quad (5)$$

This modified area factor $Z(\alpha_s)$ is graphed in Fig. 4(b). $Z(\alpha_s)$ is maximal near $\alpha_s = 6.2$ and when considering other optimization criteria 5.5 to 7 is is a practical tuning range for α_s. In particular, the maximum bucket height is obtained when the rf voltage is tuned such that α_s = 5.5 - the additional bucket height normally obtained at higher RF

ISBN 978-3-95450-173-1

voltages is eliminated by the focusing interference between the slip-stacking cavities.

For low α_s many of the losses are driven by a parametric resonance between f_s and Δf. It can be shown [21] that the resonance condition is

$$mf_s(1+\sigma) = n\Delta f$$

where the RF separation Δf is a rational multiple of the synchroton frequency f_s with a synchrotron frequency shift σ corresponding to its synchrotron oscillation amplitude ρ. In that case, the growth rate of the instability becomes

$$\ddot{\phi} \propto \rho^m \alpha_s^{-2(n-1)}$$

. Figure 5 shows the stability map for $\alpha_s = 3.6$ and depicts strong parameter resonance at the synchrotron amplitude where $f_s(1+\sigma) = 4\Delta f$.

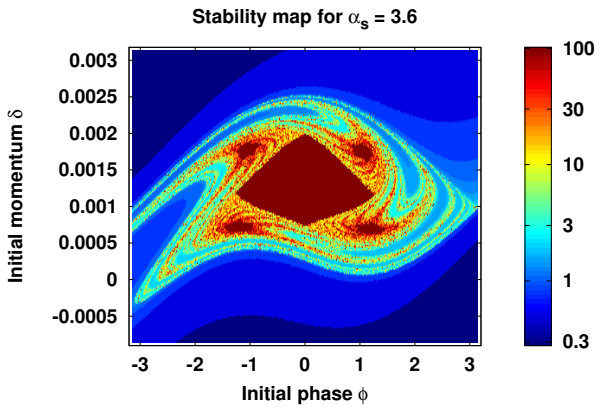

Figure 5: Stability of initial coordinates for $\alpha_s = 3.6$ (top bucket only). The color corresponds to the number of synchrotron periods a particle with the corresponding initial coordinates survives before it is lost. The four resonance islands are created by the $\omega_s(1+\sigma) = 4\omega_\phi$ parametric resonance.

INJECTION SCENARIOS AND COMPARISON OF CYCLE-RATES

These stability maps can be used to analyze injection scenarios, by weighting the (appropriately scaled) stability maps according to a distribution that represents the number of incoming particles injected into that region of phase-space. We used this technique to identify the greatest longitudinal emittance an incoming Gaussian-distributed beam could have and still achieve 97% injection efficiency at its optimal RF cavity voltage - the 97$ admittance. The longitudinal beam emittance is given in Eq. 6 below:

$$\epsilon = \pi\sigma_p\sigma_T,\ \epsilon_{97\%} = 2.17^2\pi\sigma_p\sigma_T \qquad (6)$$

The current accelerator upgrade proposal, Proton Improvement Plan II (PIP-II) [1], defines a minimum 97% slip-stacking efficiency required to maintain current loss levels while increasing intensity. Figure 6 shows the 97% admittance as a function of aspect ratio and demonstrates the consequences of a mismatched injection into a slip-stacking bucket. The optimal RF cavity voltage as a function of aspect ratio is shown in Fig. 7. Figure 8 show the slip-stacking parameter at which the injection efficiency is optimized. These results were obtaining using parameter values shown in Table. 1.

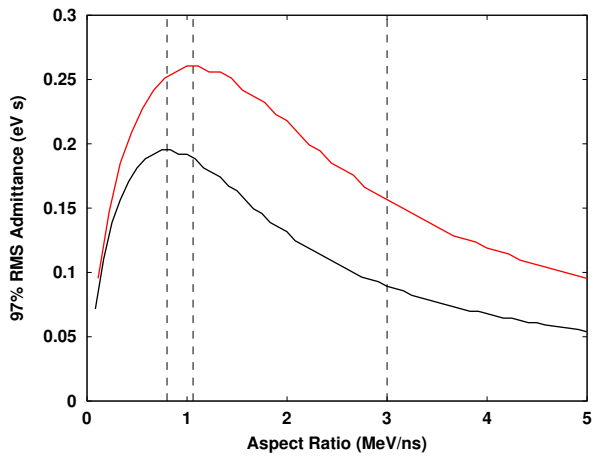

Figure 6: The 97% admittance at 97% efficiency (at an optimal value of α_s) is shown as a function of aspect ratio. The bottom line (black) is for the 15-Hz Booster cycle-rate (status quo) and top line (red) is for 20-Hz Booster cycle-rate (proposed upgrade). The vertical dashed lines represent the nominal aspect ratios given in Table 1.

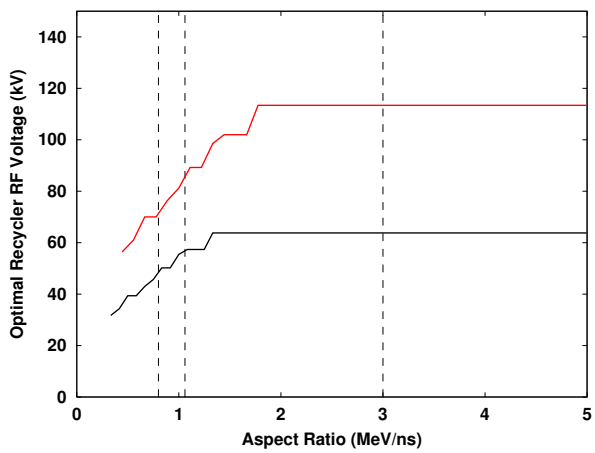

Figure 7: The optimal Recycler rf voltage for 97% admittance (at 97% efficiency) is shown as a function of aspect ratio. The bottom line (black) is for the 15-Hz Booster cycle-rate (status quo) and top line (red) is for 20-Hz Booster cycle-rate (proposed upgrade). The vertical dashed lines represent the nominal aspect ratios given in Table 1.

A nominal value for the Booster emittance is 0.12 eV·s [23]. The Fermilab Booster uses bunch rotation via quadrupole excitation [24, 25], with parameters that are

ISBN 978-3-95450-173-1

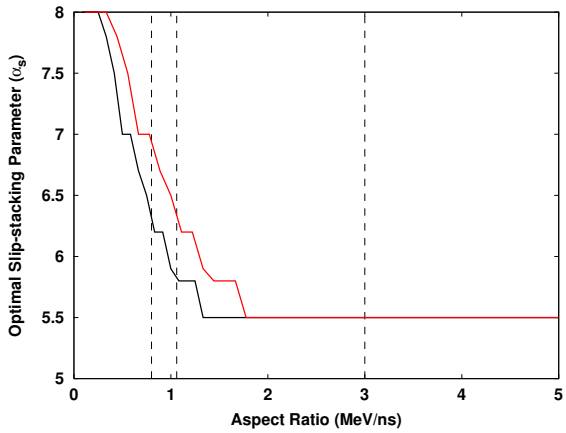

Figure 8: The optimal slip-stacking parameter α_s for 97% admittance (at 97% efficiency) is shown as a function of aspect ratio. Values of α_s greater than 8 are not evaluated. The bottom line (black) is for the 15-Hz Booster cycle-rate (status quo) and top line (red) is for 20-Hz Booster cycle-rate (proposed upgrade). The vertical dashed lines represent the nominal aspect ratios given in Table 1.

Table 2: Holding the aspect ratio and 97% efficiency constant, the 97% admittance is increased in a 20-Hz Booster.

97% Admittance	15 Hz	20 Hz
3.00 MeV/ns	0.089 eV·s	0.157 eV·s
2.00 MeV/ns	0.132 eV·s	0.218 eV·s

actively tuned to minimize losses. With bunch rotation, the aspect ratio of at least 2.6 MeV/ns is achievable at extraction from the Booster [23]. At Recycler rf cavity voltage V_0 = 100kV, the slip-stacking parameter for the Recycler is $\alpha_s(V_0) \approx 4.39$ for a 15-Hz Booster cycle-rate and $\alpha_s(V_0) \approx 5.86$ for a 20-Hz Booster cycle-rate. For other voltages, the Recycler slip-stacking parameter is given by $\alpha_s(V) = \alpha_s(V_0)\sqrt{V/V_0}$.

We examine the 97% efficiency benchmark for both a 15-Hz Booster cycle-rate and a 20-Hz Booster cycle-rate. A 20-Hz Booster cycle-rate increases the RF frequency separation by a factor of 4/3 and therefore permits a 4/3 higher bucket height (for the same level of bucket independence α_s). Consequently a 20-Hz Booster cycle-rate permits operation with either a significantly greater Booster admittance or injection efficiency. Figure 9 superimposes the Booster beam injection (natural aspect ratio without bunch rotation) for a 15-Hz Booster slip-stacking bucket and 20-Hz Booster slip-stacking bucket. Table 2 shows the improvement from a 20-Hz Booster cycle-rate expressed as a relaxation of Booster emittance limits. Table 3 shows the improvement from a 20-Hz Booster cycle-rate as greater efficiency. A 20-Hz Booster cycle-rate is clearly superior for high-intensity operation. Consequently, recent PIP-II documents have formally incorporated a 20-Hz Booster cycle rate into the specifications of the PIP-II upgrades [26].

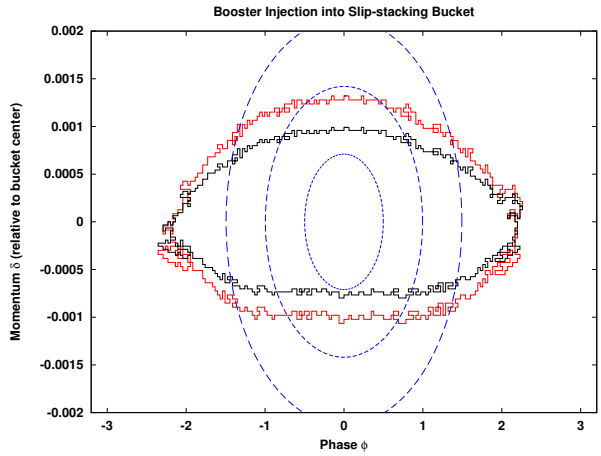

Figure 9: The shape of the slip-stacking Bucket is shown in black for the case of the 15-Hz Booster and in red for the case of the 20-Hz Booster. Both slip-stacking buckets are calculated for α_s = 5.5 and optimized for bucket height. The three dashed blue lines represent 1σ, 2σ, and 3σ of a Gaussian distribution representing a typical Booster injection. In this case, the beam emittance is 0.1 eV·s and the aspect ratio is 3 MeV/ns.

Table 3: Holding aspect ratio and emittance constant, the slip-stacking losses are dramatically reduced in a 20-Hz Booster. Bolded values pass the 97% efficiency benchmark.

Losses	15 Hz	20 Hz
with 3.00 MeV/ns & 0.08 eV·s	**2.22 %**	**0.30 %**
with 3.00 MeV/ns & 0.1 eV·s	3.97 %	**0.73 %**
with 3.00 MeV/ns & 0.12 eV·s	5.95 %	**1.38 %**
with 3.00 MeV/ns & 0.18 eV·s	12.11 %	4.29 %
with 2.00 MeV/ns & 0.08 eV·s	**0.61 %**	**0.04 %**
with 2.00 MeV/ns & 0.1 eV·s	**1.36 %**	**0.14 %**
with 2.00 MeV/ns & 0.12 eV·s	**2.39 %**	**0.33 %**
with 2.00 MeV/ns & 0.18 eV·s	6.58 %	**1.67 %**

A 20-Hz Booster would best be implemented in conjunction with a change in the slip-stacking injection scheme to avoid encountering limits in momentum aperture. Kourbanis measured the Recycler momentum aperture in May 2014 to be 0.74% for 95% transmission and 0.53% for 99% transmission [27]. It should be noted that this momentum aperture is limited by the dynamic aperture, which means that it is sensitive to chromaticity and betatron tuning; it is less than half of the physical aperture, the momentum aperture the could conceivably be achieved with improvements to the lattice (see [28]).

The total momentum range used during slip-stacking is shown in Table 4. The 20-Hz Booster requires greater RF frequency separation and therefore the total momentum used in any injection scheme would increase. However as Table 4 indicates, switching from the "On-Energy" injection with a 15-Hz Booster (status quo) to "Off-Energy" injection 20-Hz Booster (proposed) is actually a net decrease in the total

ISBN 978-3-95450-173-1

Table 4: The required momentum aperture for slip-stacking in the Recycler depending on the momentum range of the incoming beam, the injection scheme, and the Booster cycle-rate. Figures 10 and 11 depict the two injection schemes. Bolded values pass a 0.6% benchmark.

Momentum Usage	15 Hz	20 Hz
with ± 12 MeV & "On-Energy" Inj.	0.72 %	0.86 %
with ± 12 MeV & "Off-Energy" Inj.	**0.58 %**	0.67 %
with ± 8 MeV & "On-Energy" Inj.	0.63 %	0.76 %
with ± 8 MeV & "Off-Energy" Inj.	**0.48** %	**0.57** %
with ± 4 MeV & "On-Energy" Inj.	**0.52** %	0.66 %
with ± 4 MeV & "Off-Energy" Inj.	**0.38** %	**0.47** %

momentum usage. These two injection schemes are depicted in Fig. 10 and Fig. 11.

In the "On-Energy" injection scheme (see Fig. 10), the extraction energy from the Booster is the injection energy into the Recycler. The frequencies of the Recycler RF cavities move to ensure the injection and extraction is simple, but at the cost of greater momentum usage. In the "Off-Energy" injection scheme (see Fig. 11), the Recycler must be tuned to extract at a momentum $\Delta\delta/2$ lower or higher than the momentum of the beam injected into the Main Injector ([12], p. 8-109). The advantage offered by this alternate injection scheme is that only $\Delta\delta$ and the full bucket height must be accommodated, rather than the $(3/2)\Delta\delta$ and the full bucket height required by the On-Energy injection scheme. Eq. 1 relates the frequency difference with the momentum difference.

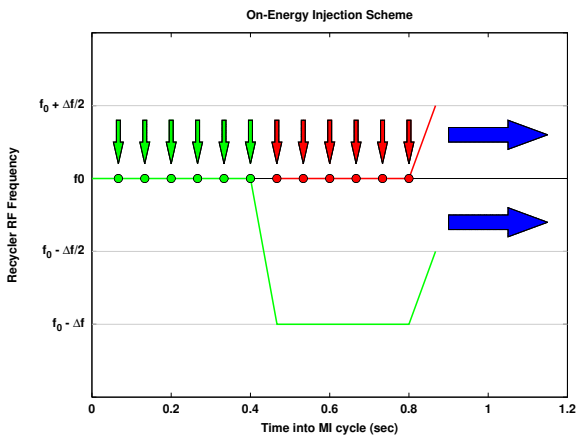

Figure 10: The On-Energy injection scheme spans the frequencies $f_0 - \Delta f$ to $f_0 + \Delta f/2$.

The gains in slip-stacking efficiency under the 20-Hz Booster scenario also require an increase in RF cavity voltage (see Fig. 7). The ideal RF cavity voltage increases from 64 kV to 114 kV, which is a factor of $(4/3)^2 \approx 1.78$. The duty factor may also decrease (by no more than 3/4) in the case of a 20-Hz Booster; the power dissipation would increase by at least $(4/3)^3 \approx 2.37$. The maximum Recycler RF voltage is 150 kV and the maximum Recycle RF power

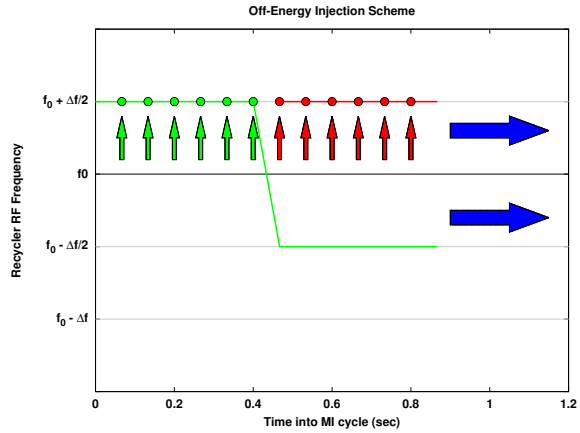

Figure 11: The Off-Energy injection scheme spans the frequencies $f_0 - \Delta f/2$ to $f_0 + \Delta f/2$.

is 150 kW, according to [16]. The possibility of the Recycler RF cavities overheating would have to be investigated.

The scaling symmetry used to analyze the 20-Hz Booster cycle-rate can generalized. An optimization at RF frequency separation Δf and aspect ratio r is equivalent to an optimization at RF frequency separation $\Delta f'$ and aspect ratio $(\Delta f'/\Delta f)r$. The same optimal slip-stacking parameter would be obtained at a higher synchrotron frequency $(\Delta f'/\Delta f)f_s$, increasing the rf voltage at $(\Delta f'/\Delta f)r$ to $(\Delta f'/\Delta f)^2 V$.

CONCLUSION

In summary, we have provided a framework for addressing both stability of particles in a slip-stacking potential. We introduce the slip-stacking area factor $F(\alpha_s)$ and the modified area factor $Z(\alpha_s)$ as tools to calculate the stable slip-stacking bucket area for any combination of accelerator parameters. We provide a general method for analyzing slip-stacking injection scenarios. We demonstrate that the 20-Hz Booster cycle rate provides a consequential improvement to the slip-stacking efficiency and bucket area. We recommend an injection scheme which wholly compensates for the the increased momentum usage required by the larger RF frequency separation. We predict the optimal RV cavity voltage for the 20-Hz Booster and identify the potential overheating issue.

REFERENCES

[1] P. Derwent et al., Proton Improvement Plan-II December 2013, 2013 [http://projectx-docdb.fnal.gov/cgi-bin/ShowDocument?docid=1232].

[2] C. Mariani (LBNE/DUSEL Collaborations), Proc. NOW 2010, [http://dx.doi.org/10.1016/j.nuclphysbps.2011.04.134].

[3] J. Galambos, M. Bai, and S. Nagaitsev, Snowmass Workshop on Frontier Capability Summary Report, 2013 [http://www.bnl.gov/swif2013/files/pdf/WorkshopSummary_Rev11.pdf].

ISBN 978-3-95450-173-1

[4] B. C. Brown, P. Adamson, D. Capista et al., Phys. Rev. ST Accel. Beams **16** , 071001 (2013) [http://dx.doi.org/10.1103/PhysRevSTAB.16.071001].

[5] F. E. Mills, Brookhaven National Laboratory Report No. 15936, 1971.

[6] D. Boussard, Y. Mizumachi, IEEE Trans. Nucl. Sci. **26**, 3623 (1979) [http://ieeexplore.ieee.org/xpls/abs_all.jsp?arnumber=4330122].

[7] J. A. MacLachlan, Fermilab Report No. FERMILAB-FN-0711, 2001 [http://lss.fnal.gov/archive/test-fn/0000/fermilab-fn-0711.pdf].

[8] K. Seiya, T. Berenc, B. Chase et al., Proc. HB2006, [www.jacow.org/abdwhb06/PAPERS/THAY02.PDF].

[9] T. Aaltonen *et al.* (CDF and D0 Collaborations), Phys. Rev. D **86**, 092003 (2012) [http://journals.aps.org/prd/abstract/10.1103/PhysRevD.86.092003].

[10] P. Adamson et al., (MINOS Collaboration), Phys. Rev. Lett. **110**, 251801 (2013) [http://journals.aps.org/prl/abstract/10.1103/PhysRevLett.110.251801].

[11] L. Fields et al., (MINERvA Collaboration), Phys. Rev. Lett. **111**, 022501 (2013) [http://journals.aps.org/prl/abstract/10.1103/PhysRevLett.111.022501].
G. A. Fiorentini et al., (MINERvA Collaboration), Phys. Rev. Lett. **111**, 022502 (2013) [http://journals.aps.org/prl/abstract/10.1103/PhysRevLett.111.022502].

[12] D. Ayres et al. (NOvA Collaboration), The NOvA Technical Design Report, FERMILAB-DESIGN-2007-01, 2007, [http://inspirehep.net/record/774999].

[13] K. Seiya *et al.*, Proc. PAC05, [http://dx.doi.org/10.1109/PAC.2005.1590430].

[14] J. Dey, K. Koba, I. Kourbanis et al., Proc. PAC01 [www.jacow.org/p01/papers/mpph048.pdf].

[15] J. Dey, I. Kourbanis, Proc. PAC05, [http://dx.doi.org/10.1109/PAC.2005.1590972].

[16] R. Madrak, D. Wildman, Proc. PAC13, [www.jacow.org/PAC2013/papers/wepma13.pdf].

[17] A. A. Aguilar-Arevalo et al. (MiniBooNE Collaboration), Phys. Rev. Lett. **98**, 231801 (2007)[http://journals.aps.org/prl/abstract/10.1103/PhysRevLett.98.231801].

[18] R. E. Ray (mu2e Collaboration), Mu2e Conceptual Design Report, 2012, [http://mu2e-docdb.fnal.gov/cgi-bin/ShowDocument?docid=1169].

[19] B. L. Roberts (New Muon (g-2) Collaboration), Chinese Physics C **34**, 741 (2010) [http://iopscience.iop.org/1674-1137/34/6/021].

[20] C. Adams et al., (LBNE Collaboration), Fermilab Report No. FERMILAB-PUB-13-438-A, 2013, [http://inspirehep.net/record/1245018].

[21] J. Eldred, R. Zwaska, Phys. Rev. ST Accel. Beams **17** , 094001 (2014) [https://journals.aps.org/prstab/pdf/10.1103/PhysRevSTAB.17.094001].

[22] H. W. Broer, I. Hoveijn, M. van Noort et al., J. Dyn. Diff. Eq. **16**, 897 (2004) [http://link.springer.com/article/10.1007%2Fs10884-004-7829-5].

[23] K. Seiya, B. Chase, J. Dey et al., Proc. BEAM07, [http://cds.cern.ch/record/1133130/files/p66.pdf]

[24] X. Yang, A. I. Drozhdin, W. Pellico, Proc. PAC07, [http://inspirehep.net/record/758224].

[25] L. A. Ahrens et al., Proc. PAC99, [www.jacow.org/p99/PAPERS/THP140.PDF].

[26] P. Derwent, S. Holmes, V. Lebedev, Fermilab Report No. BEAMS-DOC-4662-v1, 2014, [https://beamdocs.fnal.gov/AD/DocDB/0046/004662/001/THIOA05_talk.pdf].

[27] I. Kourbanis, Fermilab Report No. BEAMS-DOC-4606-v1, 2014 [https://beamdocs.fnal.gov/AD/DocDB/0046/004606/001/Doubling_MI_Power_20140520_IK.pdf].

[28] M. J. Yang, C. S. Mishra, Proc. PAC03, [www.jacow.org/p03/PAPERS/FPAB074.PDF].

ISBN 978-3-95450-173-1